

ARIES 130-cm Devasthal Fast Optical Telescope — Operation and Outcome

Y. C. Joshi^{1,*}, T. Bangia, M. K. Jaiswar, J. Pant, K. Reddy and S. Yadav

Aryabhatta Research Institute of Observational Sciences (ARIES)

Manora Peak, Nainital 263001, India

¹yogesh@aries.res.in

Received June 22, 2022; Revised November 4, 2022; Accepted November 20, 2022; Published January 20, 2023

This paper studies about the 130-cm Devasthal Fast Optical Telescope (DFOT) at Devasthal, India that has been in operation for more than 10 years and is the main workhorse for the photometric observations for a wide range of scientific programs carried out at ARIES, Nainital. Having a $2\text{k} \times 2\text{k}$ pixel imager mounted on the prime focus of the telescope, DFOT provides a field of view of about $18 \times 18 \text{ arcmin}^2$ in the sky. Another frame transfer CCD imager of 512×512 pixel size enables monitoring transient sources with millisecond temporal resolution. DFOT is equipped with a filter assembly having eight filters, an auto-guider, an All Sky Camera, and GPS-enabled weather monitoring system to support the observations in the most optimum way. The telescope is capable of producing sub-milimag photometric stability which has allowed us to detect many small-scale photometric variations.

Keywords: Telescope; instrumentation; photometric observations.

1. Introduction

Aryabhatta Research Institute of Observational Sciences (ARIES) operates a 130-cm diameter Devasthal Fast Optical Telescope (DFOT) that has been installed at Devasthal, Nainital (long = $79^\circ 41' 04''$, lat = $29^\circ 21' 40''$ N; Alt = 2420 m) in October 2010, by the DFM Engineering, Inc. USA ([Sagar et al., 2012a](#)). Devasthal is an excellent site for photometric observations from October to May when seeing is better than 1 arcsec for about 35% of the observing time with an average seeing of 1.2 ± 0.3 arcsec in a clear filter ([Stalin et al., 2001](#)). Further details on the Devasthal site can be found in [Sagar et al. \(2012b\)](#). A pictorial view of DFOT is shown in Fig. 1. The main objective of installing DFOT at Devasthal was to meet the observational requirements for the institute's core scientific interests such as monitoring of transients (gamma-ray bursts (GRBs), supernovae explosions,

extrasolar planets), variability of stars in the Milky-way, star clusters, episodic events such as active galactic nuclei and X-ray binaries, deep imaging of star clusters, the optical study of faint galaxies, etc. which otherwise solely depended on a relatively old 104-cm Sampurnanand telescope at Manora Peak, Nainital.^(a)

This paper aims to present the overall engineering aspects of the telescope. In Sec. 2, we present the telescope specification. Section 3 gives information about the detectors available on the telescope and Sec. 4 details the mechanical feature of the telescope. In Sec. 5, we present the details of filter disk assembly. The recent optical developments on the telescope are outlined in Sec. 6. Supporting instruments in the telescope house are briefly described in Sec. 7. The extinction measurement using the DFOT is presented in Sec. 8 followed by the main scientific highlight from the facility in Sec. 9. Our proposed upgradation

*Corresponding author.

^a<https://aries.res.in/facilities/astronomical-telescopes/104m-telescope>.



Fig. 1. (Color online) The on-site view of DFOT.

plans are outlined in Sec. 10. Finally, the paper is summarized in Sec. 11.

2. Telescope Specification

The telescope uses a modified Ritchey–Chretien Cassegrain design. The focal length to diameter ratio (focal ratio) of the overall telescope optics is four making it a very fast system with a plate scale of 40.05 arcsec/mm and a total field of view of 66 arcmins in diameter in the sky. The telescope mount is of a fork-equatorial type. The focus can be adjusted using a five-axis (tip, tilt, and three-axis translation) controller on the secondary mirror (M2). The telescope uses friction drives to control motions in the Right Ascension and Declination axis without any backlash. The telescope is operated through the telescope control system (TCS) which is a software system that forms the interface between the telescope's hardware and the user. The TCS consists of a mount control system, a weather station, and a PC. The TCS controls the motion of RA, DEC, M2 five-axes housing, and primary mirror (M1) doors. The weather station measures

various parameters and sends information to the TCS PC through a RS 232 serial link. The TCS also interfaces with the five-axes M2 housing, and guiding unit system. It is installed on a dedicated industrial PC with an in-built GPS card and with communication ports (TCP/IP, EXCOM, and MNCP) to communicate with the observatory control system. DFOT can operate within a Declination of -40° to $+90^{\circ}$ in the Devasthal sky.

The telescope is located 3.3-m above the ground in an open truss allowing the telescope to cool faster in the ambient condition and have a better seeing condition in comparison to the ground level platform (see Stalin *et al.*, 2001). The telescope has an open roll-of-roof type structure, designed and constructed by the institute itself. The mirrors used in the telescope are made of Corning's Ultra-Low Expansion (ULE) glass/ceramic material. The mirrors are polished where for the primary mirror, polishing accuracy of the concave optical surface is found to be 22 nm rms wavefront error at 633 nm on the useful optical surface, while the polishing accuracy of the convex optical surface was found to be 28 nm rms at 633 nm in the case of the secondary mirror. The mirrors are coated with aluminum to obtain high reflectivity at visible wavelengths. Mirrors are cleaned every year to maintain high reflectivity on their surfaces. The telescope can be pointed to a celestial object with an accuracy of 10 arcsec rms. The mechanical system is found to have a tracking accuracy of nearly 2 arcsec rms within zenith angle 0 – 40° over a 5-min period without any external guider. There is also an onsite weather monitoring system to keep a close watch on the outside weather. The telescope has two detectors for the photometric observations and is equipped with a motorized filter changer where we can keep a maximum of eight filters at any moment among broad-band Johnson–Cousin UBVRI filters, modern Sloan Digital Sky Survey (SDSS) ugriz filters, and narrow-band H-alpha, O[III], S[II] interference filters.

3. Detectors

3.1. 2048×2048 pixels CCD camera

Andor's DZ436 2048 \times 2048 array camera has $13.5 \mu\text{m}^2$ pixels and is a back-illuminated, deep thermoelectrically cooled system (-85°C) having high resolution and large dynamic range. The CCD can be read out with 31, 62, 500 and 1000 kHz speeds, with the corresponding system RMS noise of

2.5, 4.1, 6.5, 7.0 e^- and gain of 0.7, 1.4, 2.0, 2.0 e^- / ADU, respectively. The CCD chip has more than 90% quantum efficiency between 500–700 nm which decreases to about 50% at < 400 nm and > 850 nm. It has negligible dark current, low read-out noise, and high quantum efficiency, which is an ideal set up for faint imaging astronomy. Although it covers a large field of view of about 18×18 arcmin 2 area of the sky, one can also observe a smaller area of the sky through windowing which enables fast imaging with this instrument.

3.2. 512×512 pixels CCD camera

Andor's iXon EM+ DU-897 camera is an electron multiplying frame transfer back-illuminated and deep thermo-electrically cooled (-80°C) CCD imager. The CCD has a 1 MHz speed in a conventional amplifier mode with the values of readout noise from less than 1 to $49 e^-$ @10 MHz. A variable readout-dependent gain to match the 16-bit digitization can be chosen. The CCD chip has a quantum efficiency of more than 90% between 500–700 nm and falls off to 35% towards the blue end (~ 375 nm) as well as the red end (~ 950 nm). The 512×512 frame transfer CCD sensor from E2V technologies enables the charge to be multiplied on the sensor before it is read out while utilizing the full quantum efficiency performance of the CCD sensor. It covers a relatively smaller field of view of about 5.5×5.5 arcmin 2 area of the sky. This detector is most suitable for ultra-fast imaging like stellar asteroseismology where few millisecond exposures are required.

4. Mechanical Features and Telescope Enclosure

DFOT has an open truss tube design and is mounted on an equatorial fork mount. The telescope is installed on a reinforced cement concrete pier of 3.3-m in height. Pier was built by ARIES at its Devasthal site. To avoid the transfer of vibrations from the building to the telescope, a gap of 0.15 m from the pier foundation was provided. The gap provides isolation but had the possibility of back-filling with loose sand or dust over time hence gap was loosely filled with a vermiculite material. The friction drive used in the telescope provides high stiffness and smooth movement in the Right Ascension and Declination axis that facilitates good positioning and tracking of the telescope. DFOT is provided with a smooth friction drive that has a



Fig. 2. (Color online) Roll-off roof structure of 130-cm DFOT.

combination of a small roller pressed against a large disk. As there are no gears used in the drive hence the drive is without backlash and also does not require periodic lubrication.

The telescope is housed in a unique roll-off roof of size $8\text{ m} \times 8\text{ m} \times 4\text{ m}$ structure that is shown in Fig. 2. It was indigenously designed and in-house fabricated. Motorized and customized movements drive the roll-off roof and its double-walled aluminum shutters with safety interlocks. The telescope floor has a hatch opening for the transport of mirror cells and other items for performing various maintenance activities. The roof is provided with a slope of 25° to avoid the accumulation of rainwater and snow during extreme weather conditions. The outer skin of the roof has corrugated aluminum sheets, and wooden ply is provided from the inside for insulation. Limit switches, mechanical stoppers, locks, and anti-lift arrangements have been provided on the roof for safety considerations.

5. Motorized Filter Disk Controller

A motorized filter disk controller has been developed and implemented for controlling the eight positions filter disk system with the help of a stepper motor. Separate eight 1st-level LED indicators are mounted for each filter position and one 2nd-level LED indicator is mounted for all eight filter positions. For any particular valid filter position, both 2nd-level and corresponding 1st-level LED glow. Presently this system is commanded by a controller which is kept in the observing room and after reaching the requested filter position, the filter number is displayed on the display unit.

The filter disk system has linear movement in both forward and reverse directions through the lead screw linear translations mechanism. Belt pulleys are mounted on the shaft of the lead screw mechanism and stepper motor. The lead screw mechanism is rotated by the stepper motor with the help of a belt. A combination of an optical interrupter switch and an interrupter made of opaque material (aligned with each other) are mounted on the filter housing for initial referencing (homing). The interrupter switch is mounted on the fixed part and the interrupter is on the moving part of the disk. Optical filters are housed in the disk mechanism and its required positioning is obtained by rotating the disk with the help of a stepper motor. Once the system is set up and powered, the disk is continuously rotated until the home position is sensed. After homing controller keeps track of the number of steps and directions to know the exact position of the filter. The disk rotation request for homing, upward, and downward filter positions are performed by the push button switches which is displayed on the display unit. The filter disk rotates downwards or upwards depending upon whether the filter disk moves from a higher to a lower position or lower to a higher position. The number of rotations from one filter to the next filter position is 35 at the lead screw mechanism shaft. The positioning accuracy of the combined 8 filters was found to be $151\text{ }\mu\text{m}$ which is equivalent to 11 pixels in the CCD imager on the focal plane.

6. Optical Assembly

6.1. Mirror cleaning

The mirror cleaning process is carried out every year in September, just before the observing season commences after the monsoon break. The *in situ* cleaning is carried out using distilled water without unmounting the M1 and its cell. In Fig. 3, we illustrate the variation in reflectivity measurements as a function of wavelengths in the last six years, both before and after the cleaning process. It shows significant variations in the degradation of the reflectivity measurements, however, reflectivity remains almost constant after the annual cleaning. On 21 September 2022, when we carried out mirror cleaning last time, we achieved a reflectivity of almost 80% towards the blue band and 88% towards the red band after the cleaning process. In last six years, we do not see any significant drop in the

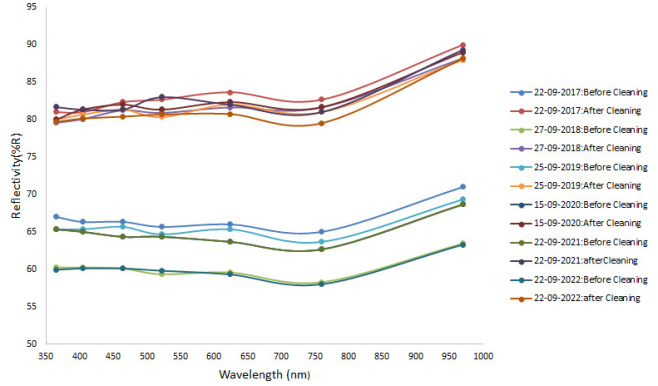


Fig. 3. (Color online) Reflectivity measurements of the M1 surface of DFOT as a function of wavelength during the period 2017–2022.

reflectivity of the primary mirror of DFOT. The corrector lens and filters are also cleaned annually along with the primary mirror using distilled water and optimal values are restored.

6.2. Telescope alignment

In the early part of the 2020 observing cycle, we noticed some issues with the M2 mounting when stellar images had shown some positional dependence which resulted in poor image quality. On thorough inspection, it was found that the spherical washer at the back plate of the M2 was dislocated from its original position. This washer set is provided for tilting the M2 during telescope alignment. The washer was fitted to its desired location and secondary was adjusted and the stability of the mount was verified. The M2 sensitivity analysis was carried out before the onset of alignment. First, the coarse optical alignment is carried out using a laser mounted at the M1 cell and a collimation mirror at the center of the M2. Alignment of M1 with respect to its cell was ensured. M2 was tilted and decentered by observing the defocused images until the inner and outer circles of defocused images become symmetric. After ensuring the M2 was focused, we measured the FWHM of the focused images which was found to be around $1.6''$. Alignment of the telescope has been carried out thereafter and image quality was revived to its original condition.

6.3. M1 radial pad gluing

In October 2018, it was observed that the M1 was shifted from its reference position. After visual inspection of the mirror radial supports, it was found that one of the radial pads of the M1 got un-glued.

To fix this issue, re-gluing of the radial pad was performed. The mirror cell was lowered down and the radial counterweight assembly was removed. Mirror was re-centered to its reference position. The Mirror surface and unglued pad were cleaned thoroughly to provide good bonding between the pad and surface. 3M Scotch-Weld™ Epoxy Adhesive 2216 with a thickness of about $300\text{ }\mu\text{m}$ was used for the gluing. The glue was allowed to cure under controlled temperature and humidity for seven days. After the gluing, the M1 was assembled and aligned with its cell. The M1 cell was then reassembled with the telescope.

7. Supporting Instruments on DFOT

7.1. All sky camera

SBIG weatherproof All Sky Camera, which measures $5.5 \times 5.5 \times 11$ inches in size ($14 \times 14 \times 28\text{ cm}$), is used for monitoring the night sky quality and measurement of sky background for the photometric data acquired with the telescope. The camera is a Monochrome KAI-0340 CCD sensor which has 640×480 pixels at $7.4\text{ }\mu\text{m}^2$, and excellent sensitivity. Protected by an acrylic dome, the Fujinon FE185C046HA-1 lens has a 1.4 mm focal length at f/1.4 and provides excellent image quality all the way to the horizon.

The All Sky has an RS-232 link to the PC for control and image download. The RS-232 link reliably downloads the full image in 15 s at 460.8 kBaud (1 kBaud = 1000 bits/s) over a 100 feet cable. Although the RS-232 interface is slower, the All Sky Camera can take an image while transmitting the previous image. Only a one second gap is required for image download, making this an excellent camera for meteor detection. The All Sky Camera, which is shown in Fig. 4, is installed on the telescope floor. The fish-eye lens is mounted to a plate that can be translated, tipped, and focused relative to the CCD Camera, so the full resolution of the lens can be achieved.

7.2. Automatic weather station

Rain Wise's MK-III-LR AWS has been used to monitor the weather on the telescope house. It provides accurate and frequent readings, has low-power requirements, and can easily record daily weather conditions. MK-III-LR features a powerful 2.4 GHz spread spectrum radio that increases range



Fig. 4. (Color online) All Sky Camera mounted on 130-cm DFOT.

to one mile in the line of site. It typically consists of a weather-proof enclosure containing the CC-3000 data logger, rechargeable battery, and meteorological sensors with an attached solar panel. Figure 5



Fig. 5. All-weather station mounted on the rooftop of 130-cm DFOT.

shows the AWS system mounted on the top of the telescope house which is connected to a separate PC in the console room. The system provides information on inside and outside temperatures, wind chill, wind speed and wind direction, humidity every minute, and measurements of rain storage every hour.

8. Sky Condition at Devasthal

The images obtained in the last five years with DFOT show the best PSF FWHM at nearly 1 arcsec and the median PSF FWHM over one year is found to be about 1.5–1.6 arcsec. The typical sky brightness at the Devasthal site is measured as 21.2 mag/arcsec² in the V band on a moonless night though it varies significantly with the phase of the moon (*Sagar et al.*, 2011). In the last five years, we obtained 150–170 photometric nights every year on this telescope where useful scientific data could be acquired. To determine the atmospheric extinction coefficients at the Devasthal sky in recent years, the absolute calibration has been carried out on a few occasions using Landolt's standard fields as reported by various authors. In Table 1, we provide extinction coefficient measurements reported by these authors during the period 2010–2018. It is evident that the extinction values vary significantly from one night to another over the different observing seasons. An average extinction estimation is calculated in the last column of the same table for five Johnson-Cousin filters where quoted error gives the mean error value. The mean atmospheric extinction coefficients measured at the DFOT site using 2k × 2k CCD Camera are estimated as 0.52 ± 0.02 , 0.26 ± 0.01 , 0.17 ± 0.01 , 0.13 ± 0.01 and 0.09 ± 0.01 mag airmass⁻¹, respectively, in U,

B, V, R_c, I_c bands.

9. Scientific Highlights

Since its inception, DFOT has been widely used for the photometric study of different kinds of celestial objects as well as monitoring the intra-night and inter-night optical variability in a variety of sources to probe the physical mechanism behind their photometric variations. Some of these studies are highlighted below.

9.1. *Transit observations of planetary systems*

The photometric monitoring of transiting exoplanets is a useful tool to characterize the planetary system as well as long-term monitoring of the exoplanetary system that may provide details of any third body that existed in the system. In one such study using transit data from DFOT for the WASP-12 system and complementing with supplementary photometric and radial velocity measurements from other facilities, *Maciejewski et al.* (2013) proposed that WASP-12b might not be the only planet in this planetary system, but there might be an additional 0.1 MJup body on a 3.6-day eccentric orbit around the host star and proposed that the two-planet system in WASP-12 is more stable on long time scales.

In the recent observations of the hot-Jupiter TrES-3b, *Mannaday et al.* (2020) carried out transit timing variation (TTV) analysis using 83 transit light curves including six from DFOT and indicated the absence of any additional planet in the system. The DFOT has also been widely used for the observations of Lunar occultations of stars (*Richichi et al.*, 2020). In one of the remarkable observations

Table 1. Extinction coefficient obtained at DFOT site in Devasthal during 2010–2018.

Filter	Extinction coefficient (mag/airmass)				
	02 Dec 2010 [1]	29 Jan 2014 [2]	21 Oct 2017 [3]	13 Jan 2018 [3]	Mean
U	—	0.558 ± 0.011	0.545 ± 0.023	0.452 ± 0.008	0.518 ± 0.015
B	0.24	0.319 ± 0.009	0.289 ± 0.011	0.198 ± 0.006	0.262 ± 0.009
V	0.14	0.216 ± 0.009	0.194 ± 0.010	0.135 ± 0.009	0.172 ± 0.009
R	—	0.148 ± 0.006	0.143 ± 0.010	0.098 ± 0.007	0.130 ± 0.008
I	0.08	0.114 ± 0.005	0.109 ± 0.012	0.064 ± 0.008	0.092 ± 0.009

Note: [1] *Sagar et al.* (2012b); [2] *Pandey et al.* (2022); [3] *Maurya & Joshi* (2020).

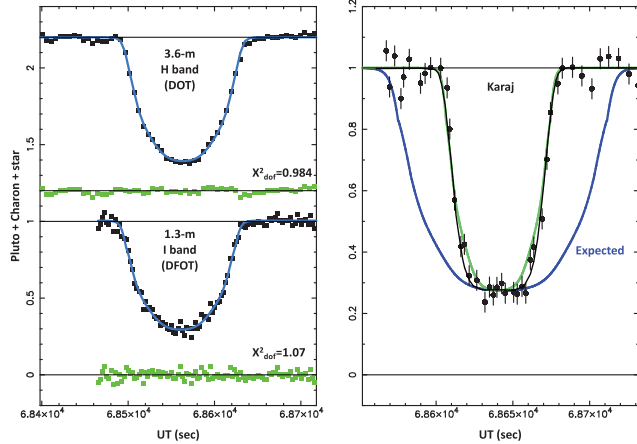


Fig. 6. (Color online) The Pluto occultation light curves obtained with the 3.6-m and 1.3-m telescopes of ARIES at Devasthal (see Sicardy *et al.*, 2021).

taken through the DFOT facility, stellar occultation by Pluto was used by Sicardy *et al.* (2021) to derive a surface pressure for Pluto’s atmosphere as $12.23^{+0.65}_{-0.38} \mu\text{bar}$ (see Fig. 6), an excellent result in agreement with the Pluto volatile transport model proposed by Meza *et al.* (2019).

9.2. Intra-night and inter-night variability in bright extragalactic sources

Multi-band intra-night and inter-night optical variability have been explored for various extragalactic sources like γ -ray-loud narrow-line Seyfert 1 galaxies (Paliya *et al.*, 2013; Ojha *et al.*, 2021), radio-quiet weak emission and broad line quasars (Chand *et al.*, 2014; Kumar *et al.*, 2015), BL Lacertae sources (Agarwal & Gupta, 2015), blazars (Mishra *et al.*, 2019; Pandey *et al.*, 2020), etc. on diverse time-scales from few hours to few months using the observations taken from the DFOT. To illustrate one such example, we show intra-day photometric variation in one of the blazar 1ES 2344 + 514 in Fig. 7 as reported by Pandey *et al.* (2020) where they found amplitudes of variability in V , R , and I bands as 40.9%, 37.4%, and 47.5%, with respective mean magnitudes of 15.25, 14.74, and 13.96 mag during six years long monitoring program at DFOT.

9.3. Follow-up monitoring of supernovae and GRBs

DFOT has been widely used to carry out qualitative analysis as well as quantitative analysis of the various transit sources through late-phase photometric

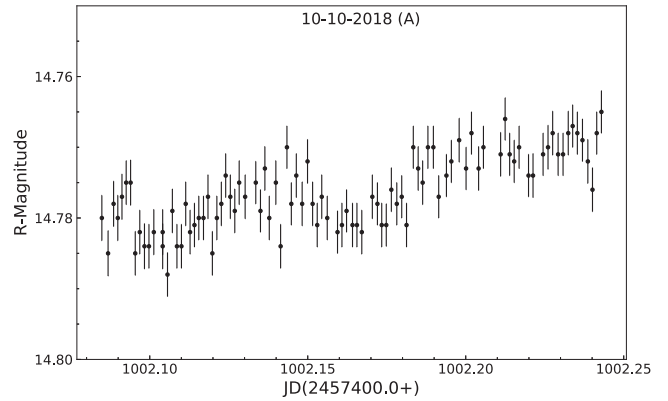


Fig. 7. The variable optical R -band intra-day variable light curve of the extreme TeV blazar 1ES 2344 + 514 (see Pandey *et al.*, 2020).

monitoring, light curve modeling, and comparison with other archetypal supernovae (Bose *et al.*, 2013, 2016; Singh *et al.*, 2018, 2019; Gangopadhyay *et al.*, 2018, 2020; Dastidar *et al.*, 2019, 2021). Extensive monitoring has been done to relate observable parameters and progenitor properties of supernovae and GRBs to understand the properties of the geometry of the explosion.

The presence of a pre-existent circumstellar medium (CSM), often associated with progenitor mass loss during the late stellar evolutionary phase, can significantly alter the observables even though originate from similar progenitors (Bose *et al.*, 2013). From the modeling of the bolometric light curves, the characteristic parameters of supernovae and GRBs like progenitor mass, radius, bolometric luminosity, and explosion energy can be derived. In one of the high-cadence multi-band photometric studies carried out by Bose *et al.* (2016) for the Type II supernovae 2014G from DFOT, they found a steep plateau slope that covers all characteristic phases of supernovae up to the radioactive tail of optical light curves, as shown in Fig. 7.

9.4. Photometric study of star clusters

It is widely believed that most stars in the Galaxy are formed in star clusters therefore their detailed study is paramount for understanding the history of star formation in the Galaxy. The photometric analysis of the cluster through the identification of genuine cluster members provides the knowledge of various cluster parameters like reddening, age, distance modulus, and photometric metallicity as well as their dynamical evolution through the determination of parameters like mass segregation,

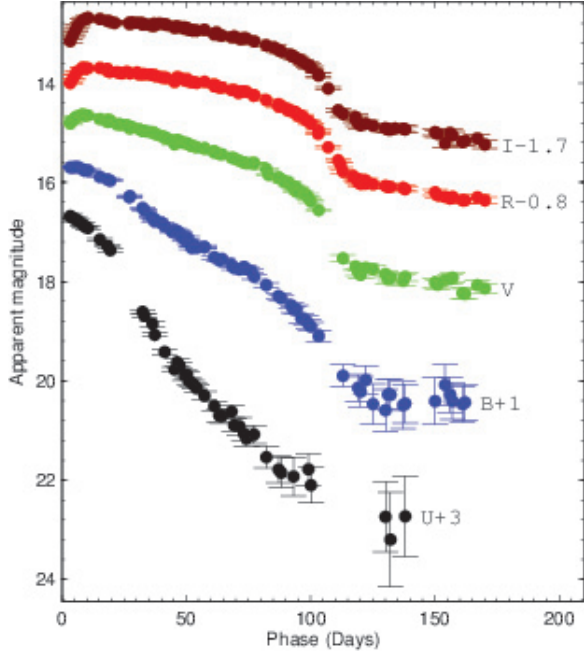


Fig. 8. (Color online) The photometric light curve of Type II supernovae 2014G in Johnson-Cousins UBVRI bands (see [Bose et al., 2016](#)).

relaxation time, and half-cluster radius ([Joshi et al., 2020a,b](#)). DFOT has been extensively used to obtain photometric data for a large range of open clusters in terms of age, richness, and galactic environments. Along with the kinematic parameters, they are probed for various photometric, kinematic, and dynamical studies ([Panwar et al., 2017](#); [Pandey et al., 2020](#)). From the optical and near-infrared color–color diagrams, the extinction values are estimated in different directions of the studied clusters. In one of the intermediate-age old open clusters SAI 45 observed through DFOT, [Maurya et al. \(2021\)](#) found the presence of an elusive extended Main-Sequence Turn-Off (eMSTO) sequence in the cluster which shows a broad Main Sequence at the brighter end (see Fig. 9) suggesting the presence of multiple star formation epochs in this cluster.

9.5. Detection of variable stars in open star clusters

Open clusters host a rich variety of variable stars and their in-depth study plays a very crucial role in understanding the intrinsic properties like pulsation, rotation, and emission of the stars. Most of the clusters host a large number of variable stars like pulsating δ Scuti and γ Dor stars, β -Ceph,

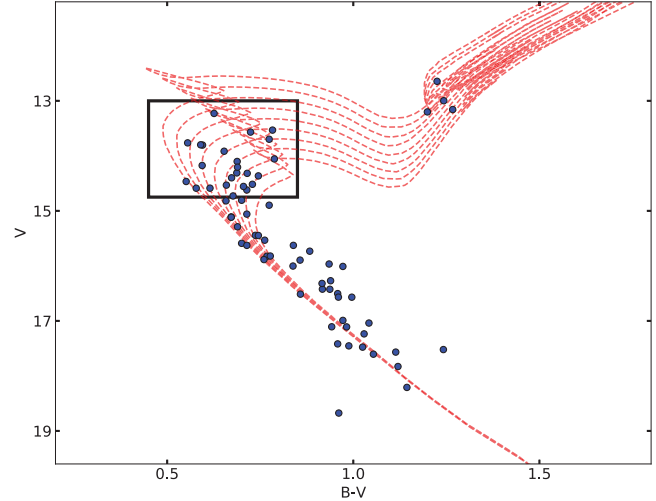


Fig. 9. (Color online) Color-magnitude diagram for SAI 45 showing eMSTO sequence towards the brighter end (see [Maurya et al., 2021](#)).

rotational variables, eclipsing binaries, etc. ([Lata et al., 2014](#); [Joshi et al., 2020a,b](#); [Sinha et al., 2020](#)). [Sinha et al. \(2020\)](#) observed star-forming region Sh 2-170 from DFOT, and reported 49 pre-main-sequence variable stars of various classes, and concluded that the stars having thicker disks rotate slower and exhibit larger photometric variations in comparison to their disk-less counterparts. In one of the most recent studies based on photometric data entirely taken from DFOT, we found 57 variables stars, including many pulsating variables in the open cluster NGC 381, some of them are shown in Fig. 10. The physical parameters like temperature, radius, and mass of these stars, are estimated through well-known empirical relations.

9.6. Photometric study of eclipsing binaries

The photometric and spectroscopic study of eclipsing binaries is useful in understanding the formation mechanism of these stars at different stages of their evolutionary phases. Even during the most illuminated moon phase period, DFOT is well suited for photometric monitoring of bright sources like Eclipsing binaries and cataclysmic variables. In the recent study by [Panchal & Joshi \(2021\)](#) and [Panchal et al. \(2022\)](#) using the data from DFOT, many W UMa eclipsing binaries have been investigated and various characteristic parameters like mass, radius, luminosity, etc. of the primary and secondary components of the selected eclipsing binaries were estimated. The long-term photometric data were also analyzed to study the change in the

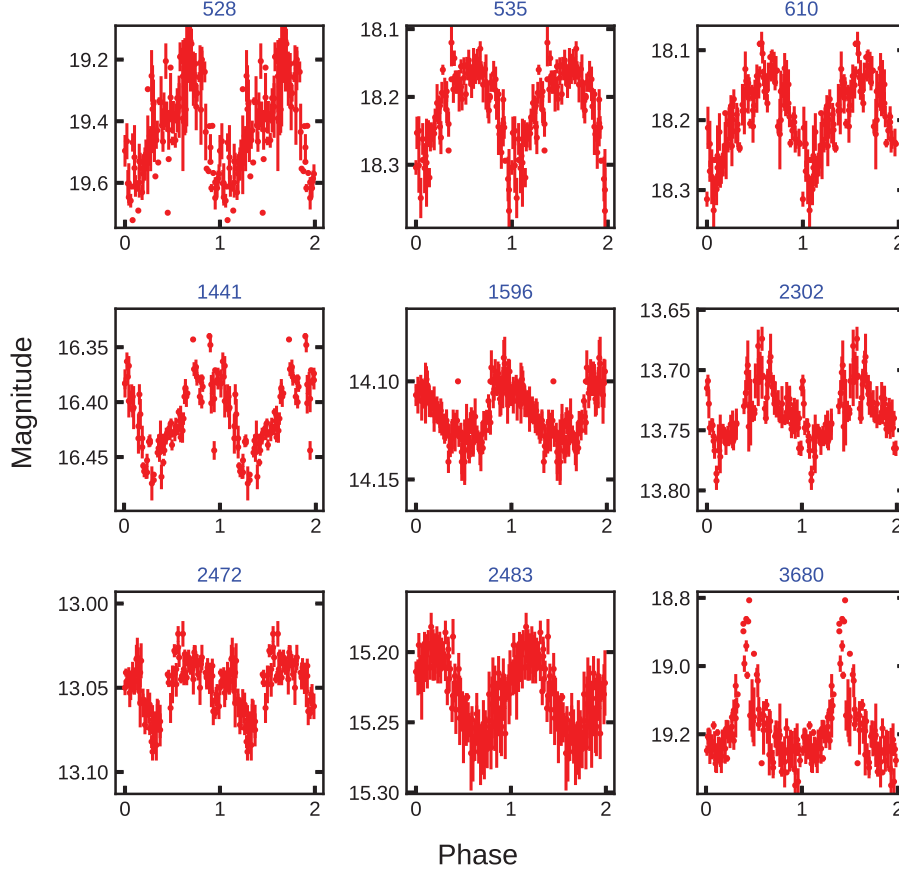


Fig. 10. (Color online) Some light curves of variable stars found in the open cluster NGC 381.

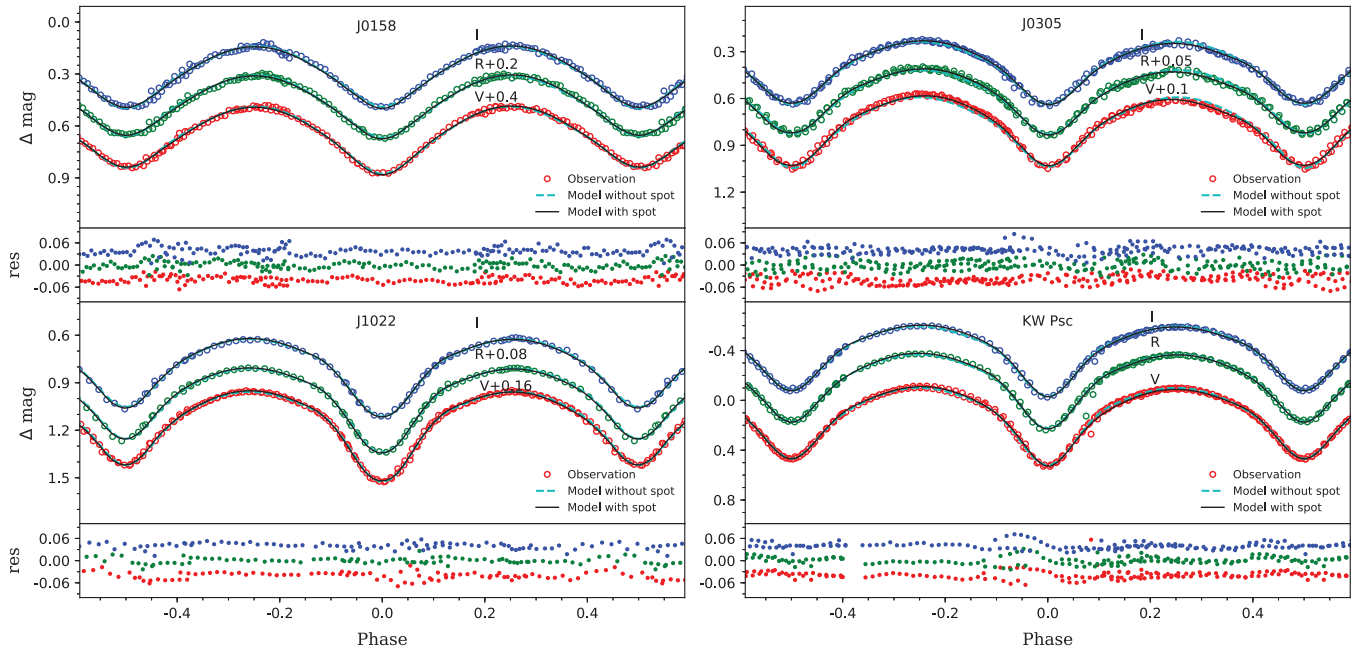


Fig. 11. (Color online) VRI light curves of four W UMa eclipsing binaries observed on the bright nights using 130-cm DFOT (Panchal & Joshi, 2021).

orbital period, mass transfer, and spot evolution in the primary and/or secondary components of these eclipsing binaries. The presence of an additional companion in the binary system and long-term cyclic magnetic activity has also been explored through the analysis of periodic variation in the ($O - C$) diagram. To illustrate one such example, we show multi-band light curves of four W UMa eclipsing binaries in Fig. 11 which were observed from DFOT. Despite monitoring these eclipsing binaries mostly on bright nights having background luminosity greater than 90%, we could extract very good stability in the photometric variations of these stars.

10. Future Upgradation Plans

As most scientific observations require fast sampling of images, we need a fast movement of filters to minimize the time lapse between two successive science observations. At present, it takes about 35 s to swap from one filter to another. We plan to have a motorized arrangement for changing the filters mounted on the filter disk of the 130-cm DFOT. The filter unit with a ball screw mechanism accommodates eight filters for observations. A filter unit with the provision for supporting the fast-changing of filters is planned in near future to facilitate the swapping of filters within 10 s. As science frames need to be taken through a set of filters repeatedly over a long period, it will reduce the dead time and increase the temporal resolution of rapidly variable sources.

A major upgrade on telescope electronics including the TCS of DFOT is also planned for the next year which will not only elevate its functioning but also make the telescope engineers and technical staff self-reliant to address the teething issues that crop up on the telescope system time to time. It is also envisaged to mount one more large-size detector in near future on DFOT like a $4\text{ k} \times 4\text{ k}$ CCD Camera with a relatively larger field of view that will further boost the scientific capabilities of this telescope.

11. Summary

Although the aperture of DFOT is small in the context of the present international scenario, the darkness and relatively good seeing at the Devasthal site make it an excellent facility for carrying out valuable astronomical research, particularly in the

field of variability study. Being its location between Australia in the East and the Canary Islands in the West, this telescope is well suited for the follow-up observations of many interesting optical transient events. In fact, the defocussing of the telescope further enables us to obtain high-precision photometry for very bright sources where we can achieve photometric stability of milli-mag rms. This telescope is well suited to do wide-field photometry like in the case of open star clusters, star-forming regions, and wide-field galaxies due to its large field of view in the sky. We also found this telescope ideally suited to detect and analyze extrasolar planets which require very high-precision photometry at the few milli-mag levels.

Acknowledgments

The authors would like to thank the scientific, engineering, and technical staff of Devasthal for their efforts to facilitate the smooth operation of the 130-cm telescope. We are also grateful to various support observers for their efficient handling of the telescope.

References

- Agarwal, A. & Gupta, A. C. [2015] *MNRAS* **450**, 541.
- Bose, S., Kumar, B. & Misra, K. [2016] *MNRAS* **455**, 2712.
- Bose, S., Kumar, B. & Sutaria, F. [2013] *MNRAS* **433**, 1871.
- Chand, H., Kumar, P. & Krishna, G. [2014] *MNRAS* **441**, 726.
- Dastidar, R., Misra, K., Singh, M. et al. [2021] *MNRAS* **504**, 1009.
- Dastidar, R., Misra, K., Valenti, S. et al. [2019] *MNRAS* **490**, 1605.
- Gangopadhyay, A., Misra, K. & Pastorello, A. [2018] *MNRAS* **476**, 3611.
- Gangopadhyay, A., Misra, K. & Sahu, D. K. [2020] *MNRAS* **497**, 3770.
- Joshi, Y. C., John, A. A., Maurya, J. et al. [2020a] *MNRAS* **499**, 618.
- Joshi, Y. C., Maurya, J., John, A. A. et al. [2020b] *MNRAS* **492**, 3602.
- Kumar, P., Krishna, G. & Chand, H. [2015] *MNRAS* **448**, 1463.
- Lata, S., Yadav, R. K. & Pandey, A. K. [2014] *MNRAS* **442**, 273.
- Maciejewski, G., Dimitrov, D., Seeliger, M. et al. [2013] *A&A* **551**, A108.
- Mannaday, V. K., Thakur, P., Ing-Guey, J. et al. [2020] *AJ* **160**, 47.
- Maurya, J. & Joshi, Y. C. [2020], *MNRAS*, **494**, 4713.
- Maurya, J., Joshi, Y. C., Elsanhoury, W. H. & Sharma, S. [2021] *AJ* **162**, 64.
- Meza, E., Sicardy, B., Assafin, M. et al. [2019] *A&A* **625**, 42.
- Mishra, S., Krishna, G., Chand, H., Chand, K. & Ojha, V. [2019] *MNRAS* **489**, 42.

- Ojha, V., Chand, H. & Gopal-Krishna [2021] *MNRAS*, **501**, 4110.
- Paliya, V. S., Stalin, C. S., Kumar, B. *et al.* [2013] *MNRAS* **428**, 2450.
- Panchal, A. & Joshi, Y. C. [2021] *AJ* **161**, 221.
- Panchal, A., Joshi, Y. C., De Cat, P. & Tiwari, S. N. [2022] *ApJ* **927**, 12.
- Pandey, R., Sharma, S., Panwar, N. *et al.* [2020] *MNRAS* **496**, 1430.
- Pandey, R., Sharma, S., Dewangan, L. K. *et al.* [2022] *ApJ* **926**, 25.
- Panwar, N., Samal, M. R., Pandey, A. K. *et al.* [2017] *MNRAS* **468**, 2684.
- Richichi, A., Sharma, S., Sinha, T. *et al.* [2020] *MNRAS* **498**, 2263.
- Sagar, R., Kumar, B., Omar, A. & Joshi, Y. C. [2012a] *BASI* **4**, 173.
- Sagar, R., Kumar, B., Omar, A. & Pandey, A. K. [2012b] *SPIE* **8444**, 1.
- Sagar, R., Omar, A., Kumar, B. *et al.* [2011] *Current Sci.* **101**, 1020.
- Sicardy, B., Ashok, N. M., Tej, A. *et al.* [2021] *ApJ* **923**, 31.
- Singh, M., Misra, K., Sahu, D. K. *et al.* [2018] *MNRAS* **474**, 2551.
- Singh, M., Misra, K., Sahu, D. K. *et al.* [2019] *MNRAS* **485**, 5438.
- Sinha, T., Sharma, S., Pandey, A. K. *et al.* [2020] *MNRAS* **493**, 267.
- Stalin, C. S., Sagar, R., Pant, P. *et al.* [2001] *BASI* **29**, 39 160, 47.